

## **Supplemental Information**

### **NAMPT-mediated NAD<sup>+</sup> biosynthesis is essential for vision in mice**

Jonathan B. Lin<sup>†</sup>, Shunsuke Kubota<sup>†</sup>, Norimitsu Ban, Mitsukuni Yoshida, Andrea Santeford, Abdoulaye Sene, Rei Nakamura, Nicole Zapata, Miyuki Kubota, Kazuo Tsubota, Jun Yoshino, Shin-ichiro Imai<sup>\*</sup>, & Rajendra S. Apte<sup>\*</sup>

<sup>†</sup> Co-first authors

<sup>\*</sup> Co-corresponding authors

### **Inventory of Supplemental Information**

Supplemental Figures S1-S7

Supplemental Experimental Procedures

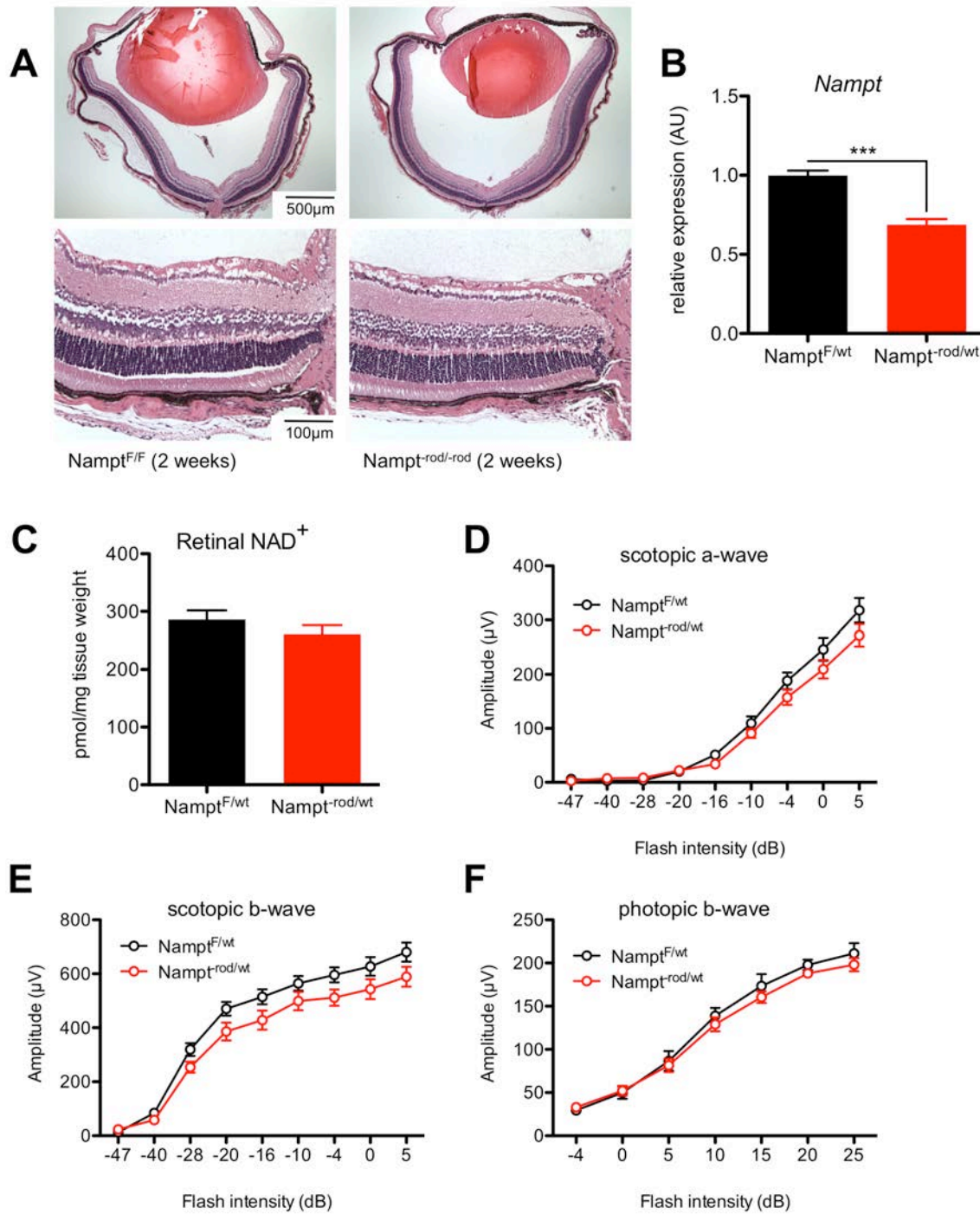


**Figure S1; Related to Figure 1.** *Nampt* expression is essential for rod photoreceptor survival. (A) Representative retinal sections at 2 weeks stained with hematoxylin & eosin showed qualitatively normal retinal appearance in *Nampt<sup>rod/rod</sup>* mice compared to *Nampt<sup>F/F</sup>* mice. Although single-allele, rod-specific deletion of *Nampt* caused significant reduction in *Nampt* expression in rod-enriched retinal isolates (B;  $n=5-6$  isolates/group; 2-tailed, unpaired t-test), this decrease in *Nampt* expression did not cause a statistically significant decrease in retinal  $\text{NAD}^+$  (C;  $n=6$  retinas/group; 2-tailed, unpaired t-test) or retinal dysfunction as measured by ERG (D-F;  $n=4$  *Nampt<sup>F/wt</sup>*/7 *Nampt<sup>rod/wt</sup>* mice; 2-way mixed ANOVA). Graphs depict mean + S.E.M. (B-C) or mean  $\pm$  S.E.M. (D-F) (\*\* $p < .001$ ).

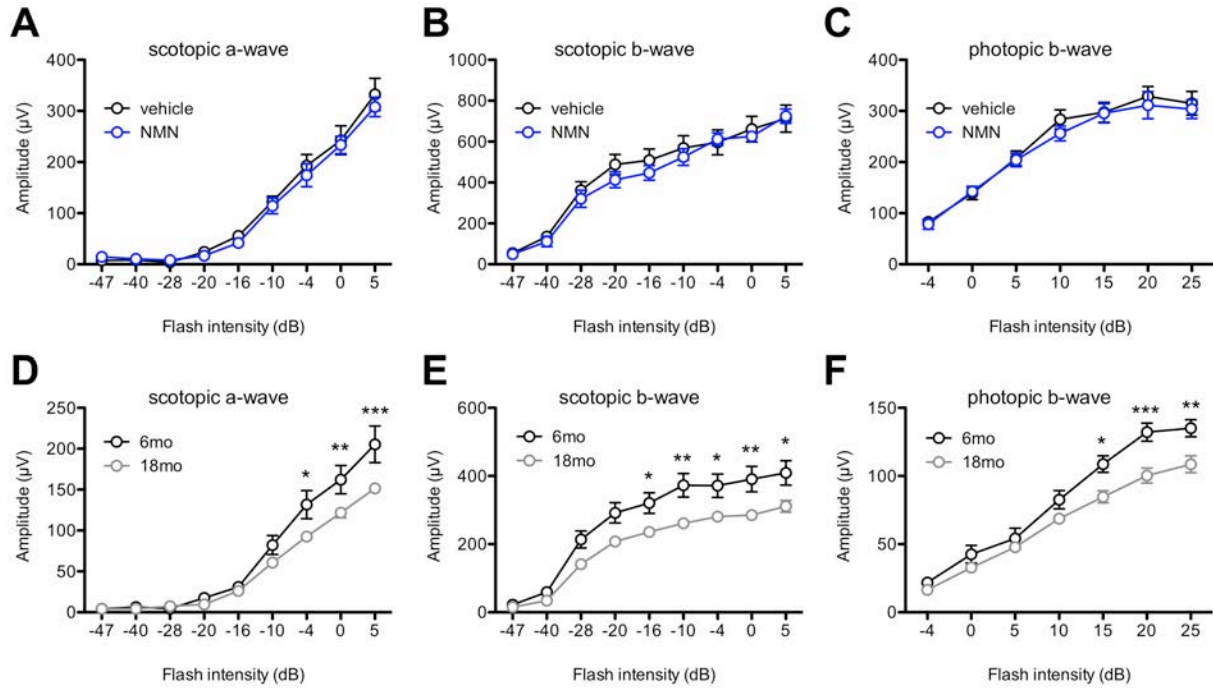


**Figure S2; Related to Figure 3.** Exogenous NMN supplementation has no effect on the retinal function of  $\text{Nampt}^{\text{F/F}}$  mice; old mice have retinal dysfunction compared to young mice. (A-C) Although daily intraperitoneal injections of 150 mg/kg NMN beginning at P5 rescued vision in  $\text{Nampt}^{\text{rod/rod}}$  and  $\text{Nampt}^{\text{cone/cone}}$  mice, they had no effect on the retinal function of  $\text{Nampt}^{\text{F/F}}$  mice by ERG ( $n=8$  vehicle/6 NMN; 2-way mixed ANOVA). (D-F) 18-month-old wild-type mice had retinal dysfunction by ERG compared to 6-month-old controls ( $n=8$  6mo/10 18mo; 2-way mixed ANOVA with Bonferroni post-hoc test). Graphs depict mean  $\pm$  S.E.M. (A-F) (\*  $p < .05$ ; \*\*  $p < .01$ ; \*\*\*  $p < .001$ ).

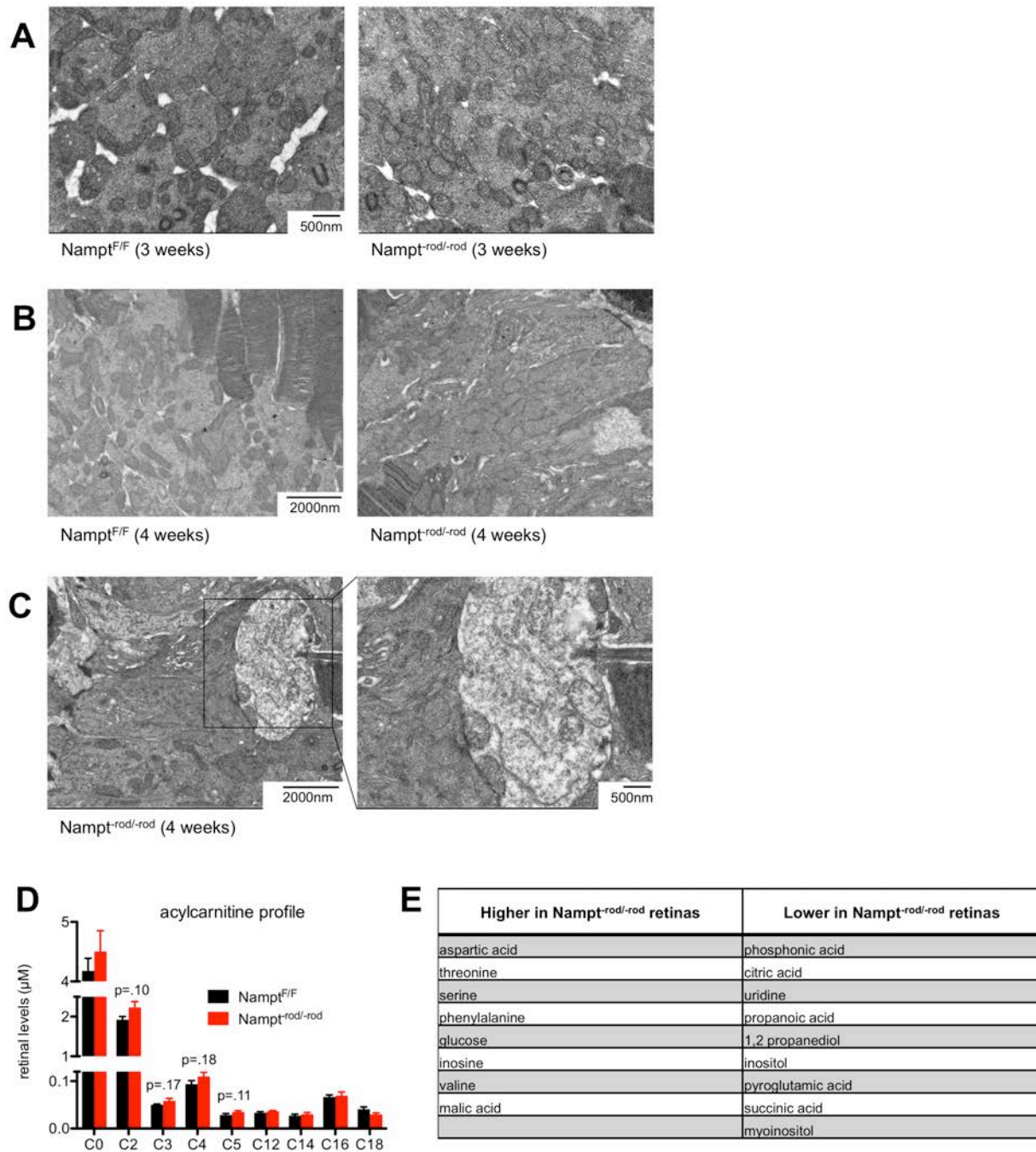


**Figure S3; Related to Figure 4.** Namp1<sup>rod/rod</sup> mice have progressive metabolic dysfunction. (A) Representative electron microscopy images of retinas from 3-week-old Namp1<sup>rod/rod</sup> mice exhibited qualitatively normal mitochondrial ultrastructure compared to images of retinas from 3-week-old Namp1<sup>F/F</sup> mice. (B) By 4 weeks, Namp1<sup>rod/rod</sup> retinas but not Namp1<sup>F/F</sup> retinas had profoundly dysmorphic photoreceptor inner segments with disruption of outer segments and (C) contained an abundance of degenerative vacuoles, which appeared to contain degenerated organelles including mitochondria with ruptured cristae. (D) Although not statistically significant, LC-MS analysis revealed trends toward accumulation of some acylcarnitines in Namp1<sup>rod/rod</sup> retinas, which are suggestive of a defect in Krebs cycle efficiency. (E) GC-MS revealed dysregulation of numerous metabolites with >1.10 fold-change between Namp1<sup>rod/rod</sup> retinas and Namp1<sup>F/F</sup> retinas (corrected p-values < .05).

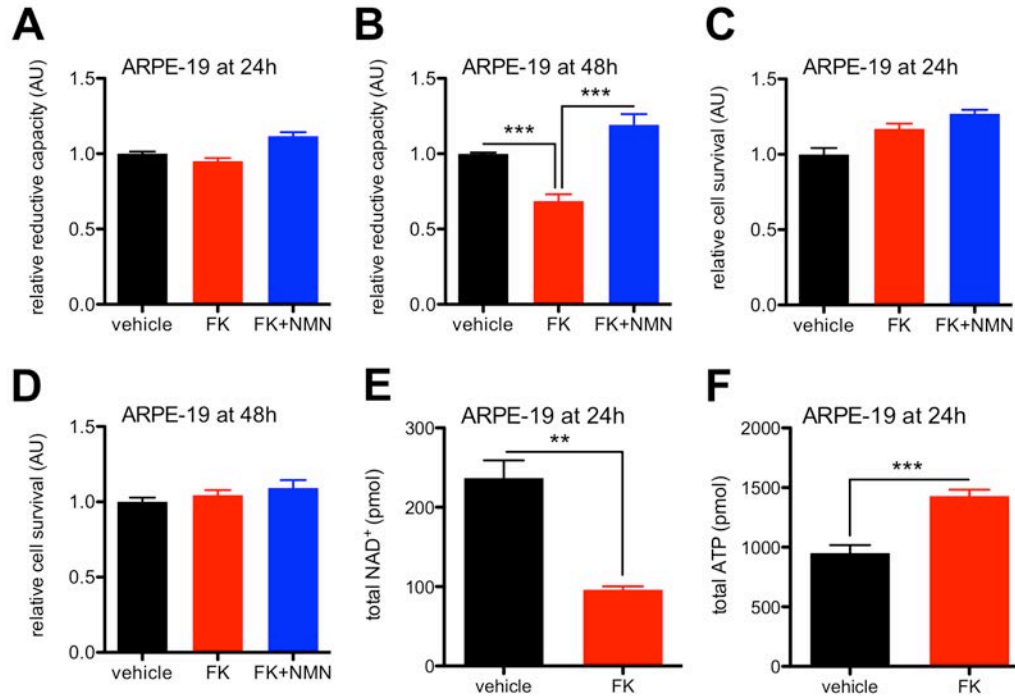


**Figure S4; Related to Figure 5.** Retinal pigment epithelium (RPE) cells are more resilient to NAMPT inhibition than photoreceptor cells. (A-B) The reductive capacity of RPE cells was unaffected by NAMPT inhibition (FK866 at 20  $\mu$ M) at 24 hours with a modest effect at 48 hours, which was rescued with 100  $\mu$ M NMN ( $n=10$ /group from two independent experiments; 1-way ANOVA with Tukey post-hoc test). (C-D) NAMPT inhibition had no effect on RPE cell survival ( $n=10$ /group from two independent experiments; 1-way ANOVA), although it did cause a reduction in total NAD<sup>+</sup> levels (E;  $n=5$ /group; 2-tailed, unpaired t-test) and a concomitant increase in total ATP levels (F;  $n=5$ /group; 2-tailed, unpaired t-test). Graphs depict mean + S.E.M. (A-F) (\*\*  $p < .01$ ; \*\*\*  $p < .001$ ).

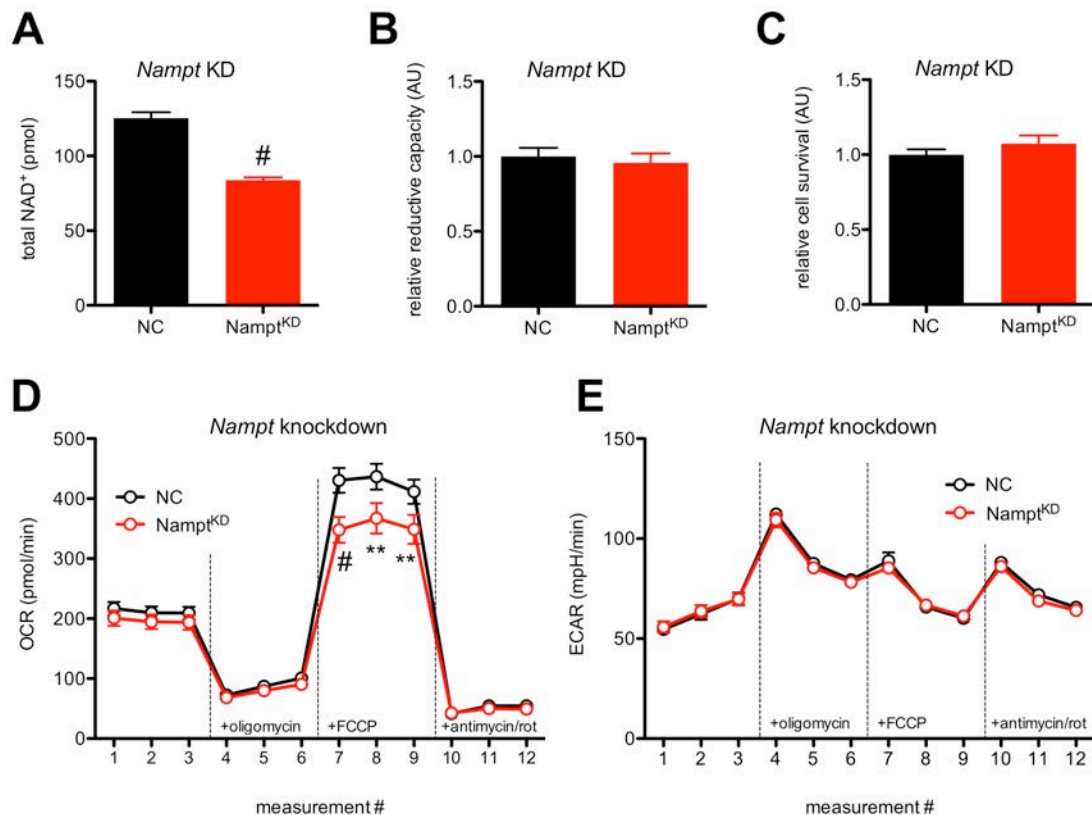


**Figure S5; Related to Figure 5.** *Nampt* knockdown (KD) in photoreceptor cells causes intermediate metabolic dysfunction. (A) *Nampt* knockdown caused significant reduction in total NAD<sup>+</sup> levels (n=6/group; 2-tailed, unpaired t-test) compared to transfection with negative control (NC) but did not affect reductive capacity (B; n=12/group from two independent experiments; Mann-Whitney U test) or cell survival (C; n=6/group; 2-tailed, unpaired t-test). (D-E) Although *Nampt* KD did not affect basal oxygen consumption rate (OCR) or basal extracellular acidification rate (ECAR), it reduced the maximal oxidative respiratory capacity, as manifested by the lower maximal OCR after FCCP treatment (n=10/group from representative experiment; 2-way mixed ANOVA with Bonferroni post-hoc test). Graphs depict mean + S.E.M. (A-C) or mean ± S.E.M. (D-E) (\*\* p < .01; # p < .0001).

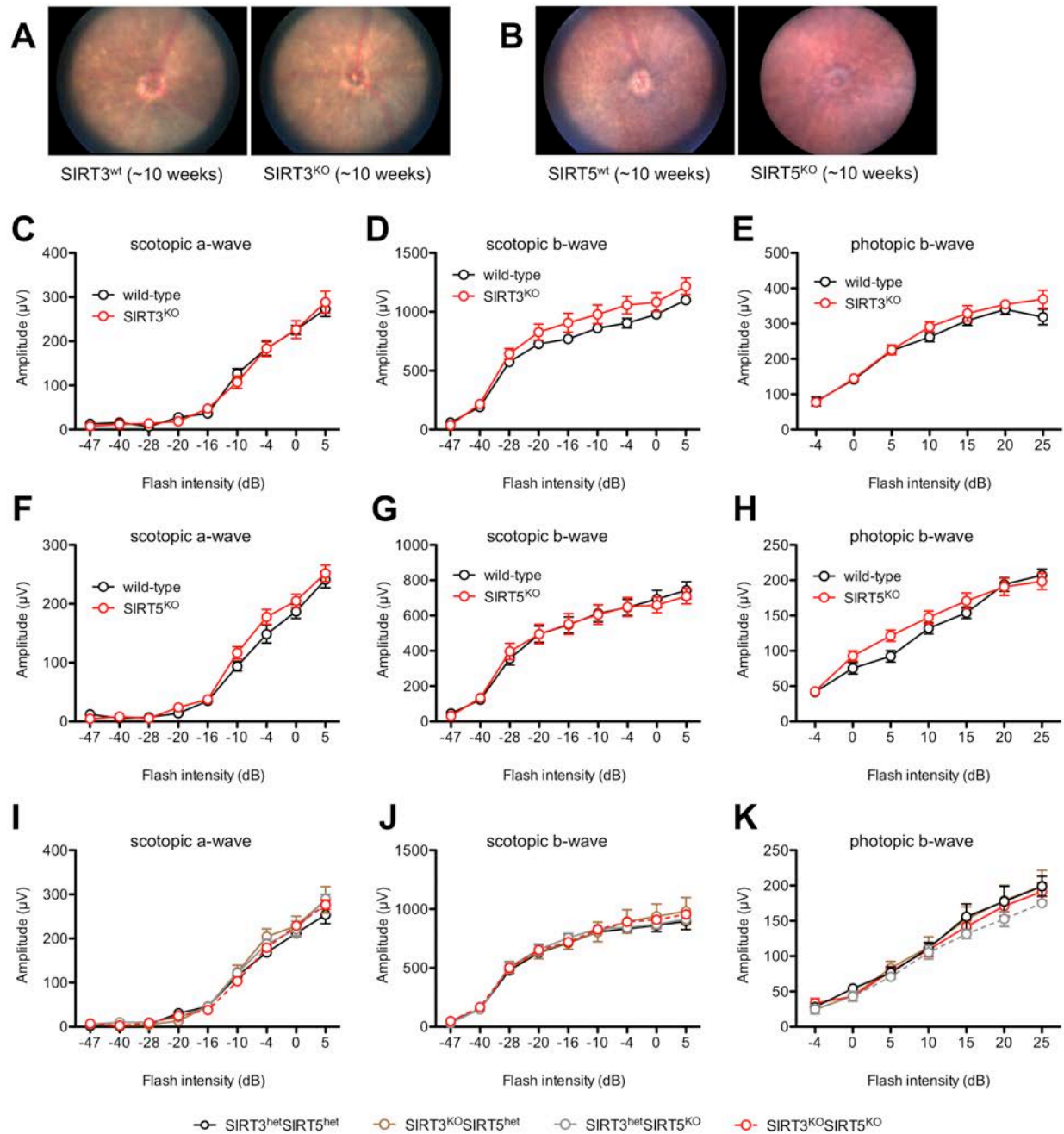


**Figure S6; Related to Figure 6.**  $SIRT3^{KO}$ ,  $SIRT5^{KO}$ , and  $SIRT3^{KO}SIRT5^{KO}$  mice have normal retinal function at baseline. (A) At 2-3 months,  $SIRT3^{KO}$  mice had a normal-appearing fundus compared to strain-matched controls and normal retinal function by ERG (C-E;  $n=5$  mice/group; 2-way mixed ANOVA). (B) At 2-3 months,  $SIRT5^{KO}$  mice also had a normal-appearing fundus compared to strain-matched controls and normal retinal function by ERG (F-H;  $n=9-10$  mice/group; 2-way mixed ANOVA). (I-K) At 2-3 months,  $SIRT3^{KO}SIRT5^{KO}$  mice had normal retinal function by ERG compared to  $SIRT3^{KO}SIRT5^{het}$ ,  $SIRT3^{het}SIRT5^{KO}$ , and  $SIRT3^{het}SIRT5^{het}$  mice ( $n=3-6$  mice/group; 2-way mixed ANOVA). Graphs depict mean  $\pm$  S.E.M. (C-K).

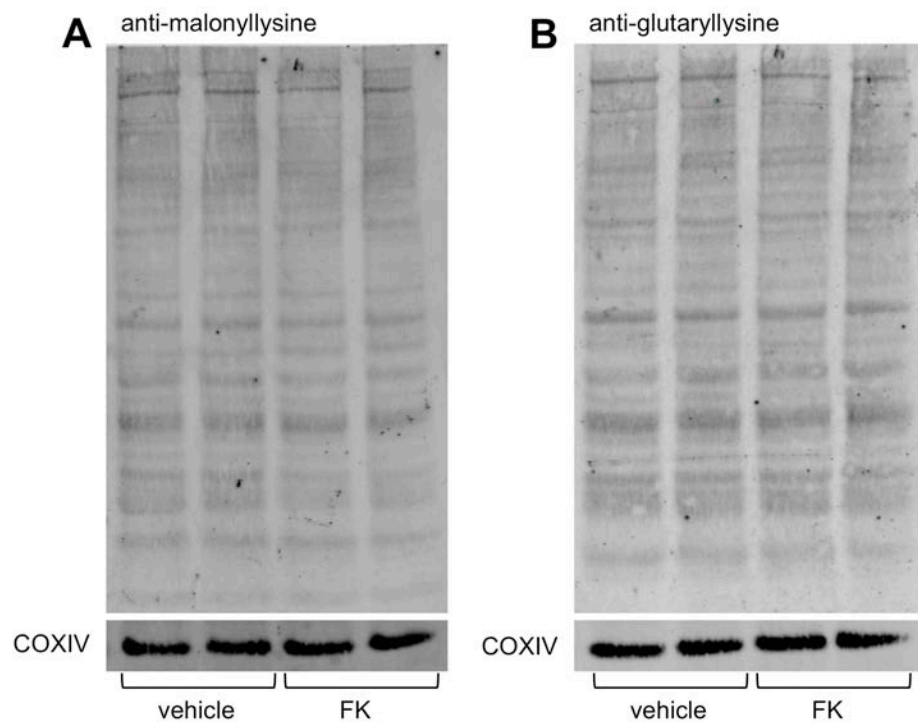


**Figure S7; Related to Figure 7.** NAMPT inhibition does not affect the malonylation and glutarylation profile of mitochondrial proteins in photoreceptor cells. Malonylation (A) and glutarylation (B) of mitochondrial proteins was unchanged in photoreceptor cells after NAMPT inhibition (representative blots showing 2 biological replicates).

## SUPPLEMENTAL EXPERIMENTAL PROCEDURES

### Immunohistochemistry

For NAMPT and cone arrestin co-immunofluorescence, we de-paraffinized slides in 100% xylene, rehydrated them through graded ethanol solutions, and subjected them to antigen retrieval for 3 minutes in a decloaking chamber (BioCare Medical, Concord CA) using a citrate-based antigen unmasking solution (Vector Labs, Burlingame CA). After cooling, we washed slides in running diH<sub>2</sub>O and 3 changes of PBS, blocked non-specific binding with the included blocking solution for 30 minutes at room temperature, and stained them with a 1:10,000 dilution of rabbit anti-NAMPT(161-173) primary antibody (B5812-200UL; Sigma, St. Louis MO) overnight at 4°C in a humidified chamber. The next day, we washed slides and incubated them in a 1:200 dilution of HRP-conjugated donkey anti-rabbit secondary for 60 minutes at room temperature. After washing in PBS, we developed the signal with Alexa Fluor 546 tyramide in 0.3% H<sub>2</sub>O<sub>2</sub> in amplification buffer (Life Technologies, Grand Island NY) for 7 minutes. We then washed slides again in PBS, subjected them to antigen retrieval and blocking as above, and incubated with rabbit anti-cone arrestin (AB15282; Millipore, Billerica MA) at a 1:500 dilution overnight at 4°C. We washed the slides in PBS and applied Alexa Fluor 488 goat anti-rabbit secondary antibody at a 1:400 dilution for 60 minutes followed by additional PBS washes. Finally, we mounted the slides with ProLong Gold antifade reagent with DAPI (Life Technologies, Grand Island NY).

### Electroretinography

We used the UTAS-E3000 Visual Electrodiagnostic System running EM for Windows (LKC Technologies, Gaithersburg MD). After dark adaptation overnight, we anesthetized the mice with 86.9 mg/kg ketamine and 13.4 mg/kg xylazine, dilated the pupils with 1.0% atropine sulfate (Bausch & Lomb, Tampa FL), and placed electrodes under dim red illumination. The recording electrode was a platinum loop of 2.0 mm diameter and was positioned in a drop of 1.25% hydroxypropyl methylcellulose (GONAK; Akorn, Buffalo Grove IL) on the cornea of each eye. The reference electrode was inserted under the skin at the vertex of the skull, while the ground electrode was inserted under the skin of the back near the tail. We maintained the body temperature of the mice at  $37.5 \pm 1.0^\circ\text{C}$  with a heating pad controlled by a rectal temperature probe (FHC, Bowdoin ME). For testing, we positioned the head just inside the opening of the Ganzfeld dome. The stimulus for each trial consisted of a brief (10 ms) full-field flash either in darkness or in the presence of dim background illumination (30.0 cd/m<sup>2</sup>) after 10 minutes of adaptation to the background light. We recorded the electrical retinal response beginning 25 ms prior to the flash and ending 250 ms after the flash. We averaged the responses from several trials for each light intensity.

### Photopic visual acuity

Briefly, the OptoMotry System consists of a square array of four computer monitors surrounding a central pedestal where the mouse is placed. A video camera is mounted above the pedestal to allow for observation of the mouse. During each trial, rotating sine-wave vertical gratings of 100% contrast are displayed on the monitors to form a virtual cylinder around the mouse that rotates either clockwise or counterclockwise. Mice respond to these stimuli by reflexively rotating their head in the corresponding direction. The rotation direction for each 5 s trial was randomly selected by a computer program. An observer blinded to the rotation direction and to the mouse genotype indicated the perceived direction of mouse head motion (clockwise or counterclockwise). Using the staircase paradigm, the computer program adjusted the spatial frequency (Fs) of the stimuli based on whether the previous response was correct, beginning with 0.128 cycles per degree and ending at maximal visual acuity (i.e., 70% correct responses). We set the speed of gratings (Sp) to its optimal value (12.0°/s) (Kolesnikov et al., 2011; Umino et al., 2008) and allowed the computer program to automatically adjust the temporal frequency (Ft).

### Quantification of NAD<sup>+</sup> & ATP levels with HPLC

We homogenized snap-frozen samples in perchloric acid and then neutralized extracts with potassium carbonate on ice. For NAD<sup>+</sup>/ATP measurements, we ran the HPLC at a flow rate of 1 ml/min with 100% buffer A (0.05 M phosphate buffer) from 0-5 min, a linear gradient to 95% buffer A/5% buffer B (100% methanol) from 5-6 min, 95% buffer A/5% buffer B from 6-11 min, a linear gradient to 85% buffer A/15% buffer B from 11-13 min, 85% buffer A/15% buffer B from 13-23 min, a linear gradient to 100% buffer A from 23-24 min, and 100% buffer A from 24-30 min. We further analyzed and confirmed NAD<sup>+</sup> fractions from HPLC with LC/MS/MS.